doi.org/10.36721/PJPS.2020.33.1.REG.109-119.1

Hyaluronic acid-coated nanostructured lipid carriers for loading multiple traditional Chinese medicine components for liver cancer treatment

Shuang Sun[1], Qingxia Guan[1], Eryu Shang[2], Hongbin Xiao[1], Xin Yu[1], Lei Shi[1], Chengcheng Zhao[1], Yuyan Guo[1] , Shaowa Lv[1] and Yongji Li[1*]

[1]College of Pharmacy, Heilongjiang University of Chinese Medicine, Harbin, China
[2]Fire Control Room, Heilongjiang Forest Protection Institute, Harbin, China

Abstract: This study aimed to develop hyaluronic acid (HA)-coated nanostructured lipid carriers (NLC) loaded simultaneously with oleanolic acid (OA), ursolic acid (UA) and Ginsenoside Rg3 (Rg3), prepared by electrostatic attraction for delivering OA, UA and Rg3 (OUR), termed HA-OUR-NLC, to tumors over expressing cluster determinant 44(CD44). The dialysis method was used to assess the *in vitro* release of OUR. Parameters such as pharmacokinetics, biodistribution, fluorescence *in vivo* endo-microscopy (FIVE), optical *in vivo* imaging (OIVI) data, and *in vivo* antitumor effects were evaluated. The results showed a total drug loading rate of 8.76±0.95% for the optimized HA-OUR-NLC; total encapsulation efficiency was 45.67±1.14%; particle size was 165.15±3.84%; polydispersity index was 0.227±0.01; zeta potential was -22.87±0.97 mV. Drug release followed the Higuchi kinetics. Pharmacokinetics and tissue distribution, as well as antitumor effects were evaluated in nude mice *in vivo*. HA-OUR-NLC were better tolerated, with increased antitumor activity compared with 5-Fu. In *in vivo* optical imaging, we use 1,1'-dioctadecyl-3,3,3',3'-tetramethy(DiR) as a fluorescent dye to label the NLC. The DiR-OUR-NLC group showed bright systemic signals, while the tumor site was weak. The present findings indicated that HA-OUR-NLC accumulated in the tumor site, prolonging OUR duration in the circulation and enhancing tumoral concentrations. Therefore, NLC prepared by electrostatic attraction constitute a good system for delivering OUR to tumors.

Keywords: Nanostructured lipid carriers, multiple components, Hyaluronic acid, CD44, Tumor target, Fluorescence *in vivo* endo-microscopy (FIVE)

INTRODUCTION

Ginseng (*Panax ginseng* C.A. Meyer) has been used as a traditional precious herb in China for thousands of years, which belongs to araliaceae ginseng species. It has noticeable effects in protecting the liver and elevating immune function (Igami *et al.*, 2015; Niranjana Murthy *et al.*, 2014; Oh *et al.*, 2015). Previous studies have demonstrated that ginseng's major bioactive components (ginsenosides Rg3) have complex structures and multifaceted pharmacological functions, including anticancer properties (Helms, 2004; Wang *et al.*, 2007). Meanwhile, ginseng shows anticarcinogenic effects on transplanted tumors and cultured hepatoma cells, in animal and human cancers (Wu *et al.*, 2001). OA and its isomer UA are also ginseng components, and have been used successfully to treat liver cancer. In a report by Yu-Ying Han, OA and UA were shown to inhibit the proliferation of malignantly transformed WB-F344 cells, which may reflect the anti-tumor effects of OA and UA (Han *et al.*, 2014). However, these three active ingredients are limited by poor solubility. Because of strong hydrophobicity, the therapeutic effects of OA might not be satisfactory in *vivo*; indeed, its biological activity and bioavailability are limited.

A strategy for overcoming the poor solubility and increasing *in vivo* efficacy of OA, UA and Rg3 is to encapsulate these three components in nanoparticles; this would increase their therapeutic effects and in *vivo* release characteristics (Zhang *et al.*, 2013).

Nanostructured lipid carriers (NLC), a new generation of solid lipid nanoparticles (SLN), consist of a solid lipid matrix with certain amounts of soluble lipids, which increases drug loading results due to imperfections in crystal structure (Liu *et al.*, 2011b).

NLC drug delivery systems have several advantages in cancer therapy, including good biocompatibility, high drug loading capacity, controllable drug release, high stability during storage, and upscaling feasibility (Luan *et al.*, 2014; Shamma and Aburahma, 2014; Yang *et al.*, 2013).

In recent years, multiple molecules have been applied to target antitumor drugs to the tumor, e.g. biotin, folic acid, and HA (Danhier *et al.*, 2009; De Stefano *et al.*, 2011; Heo *et al.*, 2012; Zhan *et al.*, 2010; Zhao *et al.*, 2010). Of these, HA has been widely assessed thanks to its unique characteristics.

**Corresponding author:* e-mail: 309642421@qq.com

CD44 is an extra cellular protein on the cytoplasmic membrane. HA is one of the main peri-cellular matrix components. It binds to CD44 specifically, and is responsible for cell-mediated responses. CD44 is rarely expressed in normal tissues. Therefore, HA and CD44 combination provides a new prospect for tumor targeting.

The main purpose of this study was to develop a new tumor targeting delivery system: HA-coated nanostructured lipid carriers loaded simultaneously with OUR (HA-OUR-NLC), obtained by electrostatic attraction for OUR delivery to tumors. First, the preparation and characterization of cationic OUR-NLC were assessed. Secondly, HA-OUR-NLC were prepared with HA, selected as the target molecule. Finally, pharmacokinetic parameters and targeting properties were evaluated by biodistribution, Fluorescence *In Vivo* Endomicroscopy (FIVE) and Optical *In vivo* Imaging (OIVI).

MATERIALS AND METHODS

OA' UA' and Rg3 were provided by Chengdu Jin Zhe Biological Co., Ltd (batch numbers 130826, 131107, and 131029, respectively). CTAB was provided by Big Alum Chemical Reagent Factory in Tianjin (China). HA was purchased from Nanjing Zelang Biochem Co., Ltd. (China). The remaining chemicals were of analytical grade. Dialysis bags were purchased from Sigma (St. Louis, MO, USA). SMMC-7721 cells were purchased from Shanghai Bogoo Biochem Co Ltd. (China).

Instruments

Ultrasonic cell disruptor (VCX750, Sonics, USA). Malvern Zetasizer 3000 (Malvern, Worcestershire, UK). Transmission electron microscopy (model TECNAIG2, Philips, Eindhoven, The Netherlands).

OUR-NLC preparation

OUR-NLC were prepared by the solvent ultrasonic dispersion method. Oleic acid and glyceryl monostearate were applied in NLC, as previously reported (Wang *et al.*, 2010).

The amounts of OA, UA, and Rg3 used in this study were all 2 g. Briefly, the desired amounts of oleic acid, glyceryl monostearate and OUR were dissolved in 5 ml ethanol in a water bath at 60^{o}C. Then, the organic phase was slowly added to 30ml distilled water with agitation and evaporated under vacuum. The mixture was dispersed in 50 ml of 0.1% CTAB (w/v) solution using ultrasonic cell breaking for 20 min, and stirred magnetically at 80^{o}C (30 r/min) for emulsification. Finally, OUR-NLC were obtained.

HA-OUR-NLC preparation

We used the electrostatic attraction method to prepare HA-OUR-NLC. The desired volume of OUR-NLC dispersion was added to the HA solution under vigorous stirring at a concentration of 0.10%, 0.50%, 1.00%, 1.50% or 2.00% wt. HA concentration, HA to OUR-NLC mass ratio, and stirring rate were assessed to obtain the best prescription.

Nanoparticle characteristics

Particle size and zeta potential of the HA-OUR-NLC were measured on a Malvern Zetasizer 300. The polydispersity index was used to quantify particle size distribution. The HA-OUR-NLC were diluted prior to particle size and zeta potential determination (Yang *et al.*, 2007).

Transmission electron microscopy

The morphology of HA-OUR-NLC was determined by transmission electron microscopy (TEM) (Zhang *et al.*, 2013). For TEM studies, an HA-OUR-NLC sample was placed on copper in 2% aqueous solution of sodium phospho-tungstate for 2-3 mins.

In vitro release

First, OA, UA and Rg3 release from OUR-NLC was carried out by dialysis in bags soaked in double-distilled water for 12h. Then, lyophilized suspensions of OUR-NLC were added to dialysis bags, in turn placed in 50 mL PBS (pH 7.4). At regular time intervals, 1 ml of the release medium was collected, and fresh release medium filled to maintain a constant volume (Jain *et al.*, 2012). Control experiments were performed the same way with the same proportions of OA, UA and Rg3 as in OUR-NLC, to evaluate drug release behavior.

Pharmacokinetic assessment and tissue distribution

SMMC-7721-bearing female BALB/C-nu nude mice (18-22g) with tumors of 0-200 mm^3 at 3-6 weeks after cancer cell transplantation were randomly divided into three groups, including (1) OUR, (2) OUR-NLC, and (3) HA-OUR-NLC groups. Each group was injected the above formulations at 10 mg/kg via the caudal vein; blood was collected by retro-orbital bleeding at 10 min, 0.5h, 1h, 2h, and 3h and stored (n=6). After sacrifice, the heart, kidney, spleen, liver, lung and tumor were collected to determine the amounts of OA, UA and Rg3. Each tissue was first weighed and homogenized in physiological saline. The three constituents were extracted with acetonitrile (3 ml), and centrifuged (10,000 rpm, 5 min). The resulting supernatant was collected, and OUR levels were determined by HPLC as described above. The following formulas were used (Liu *et al.*, 2011a):

Maximum concentrations (Ce) = $(C_{max})_{NLC}/(C_{max})_{solution}$ (1)

Relative uptake efficiency (RUE)=$AUC_{NLC}/AUC_{solution}$ (2)

Relative targeting efficiency (RTE) = $[(AUC_{tissue}/AUC_{sum})_{NLC}-(AUC_{tissue}/AUC_{sum})_{solution}]/(AUC_{tissue}/AUC_{sum})_{solution}$ (3)

where AUC is the area under the concentration–time curve in each issue;

AUC_{sum} is the sum of AUC values in the heart, liver, spleen, lung, kidney and tumor; AUC_{tissue} is the area under the concentration–time curve in each tissue after HA-OUR-NLC administration; $AUC_{solution}$ is the area under the concentration-time curve in each tissue after drug administration; AUC_{NLC} is the area under the concentration–time curve in each tissue after NLC administration; $(Cmax)_{solution}$ is the maximum concentration of OA, UA or Rg3 in each tissue after NLC administration; $(Cmax)_{solution}$ is the maximum concentration of OA, UA or Rg3 in each tissue after drug administration.

Fluorescence in vivo endomicroscopy

Eighteen SMMC-7721-bearing female BALB/C-nu nude mice were divided into three groups, including FITC-OUR-NLC, FITC-HA-OUR-NLC and FITC groups. Before the experiments, the nude mice were fasted for 12h with water allowed. The mice were deeply anaesthetized with pentobarbital sodium (2%) i.p. and by caudal vein injection at 10 mg/kg of drug (0.1 mL/20 g). The probe was placed in the liver and tumor, and images were acquired at 5 min, 15 min, 30 min, 1h, 2h and 4h for each group.

Optical in vivo imaging

DIR was used as a fluorescent dye to label the NLC and investigate initial targeting efficiency. Eighteen SMMC-7721-bearing female BALB/C-nu nude mice were divided into three groups, including DIR-OUR-NLC, DIR-HA-OUR-NLC and DIR groups. The animals were treated as in 2.8. Nude mice were placed in Optical *in Vivo* Imaging to acquire images at 10 min, 0.5h, 1h, 2h, 3h and 12h.

In vivo antitumor efficacy

SMMC-7721-bearing female BALB/C-nu nude mice weighing 18-22 g were supplied by the Beijing Weitong Lihua company. Animal experiments were performed according to the requirements of the National Act on the Use of Experimental Animals (PR China), and approved by the Animal Ethics Committee of Heilongjiang University of Chinese Medicine.

SMMC-7721-bearing female BALB/C-nu nude mice (18-22 g) were injected subcutaneously on the right shoulder with 0.2 ml of cell suspension containing about 10^7 SMMC-7721 cells (Chen *et al.*, 2012; Li *et al.*, 2016; Li *et al.*, 2016). After 3-6 weeks, obvious solid tumors could be observed. When the solid tumors reached 0-100 mm^3 in volume, SMMC-7721-bearing female BALB/C-nu nude mice were divided into five groups (5 per group), including (1) physiological saline (N.S), (2) 5-Fu (500 g/m^2), (3) HA-OUR-NLC (0.3 mg/kg), (4) OUR-NLC (0.3 mg/kg), and (5) OUR solution (0.3 mg/kg) groups.

The animals were treated with respective formulations by intraperitoneal injection. Specifically, group (1)' (3)' (4)' and (5) animals were injected daily for 21 days; group (2) mice were injected weekly for three weeks.

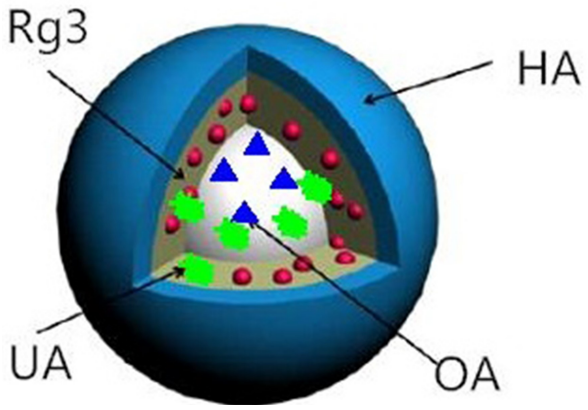

Fig. 1: Encapsulation of HA-OUR-NLC using the solvent ultrasonic dispersion method.

Solid tumor diameters were measured by calipers; mouse weights were measured every other day. Finally, the animals were sacrificed, and the tumors excised and weighed on an electronic balance. Tumor volumes were derived using the following formula (Liu et al., 2011a):

$V=1/2ab^2$

where a is the longest diameter and b is the shortest diameter. In addition, H&E staining and CD34 immunohisto chemistry were used to assess *in vivo* antitumor efficacy.

RESULTS

Preparation of OUR-NLC and HA-OUR-NLC

The OUR-NLC were successfully obtained by the solvent ultrasonic dispersion method (fig. 1).

Physicochemical characterization of HA-OUR-NLC

The HA-OUR-NLC were prepared according to formulation factors predicted by the central composite design. Average particle size was 165.15±3.84 nm, with a polydispersity index of 0.22±0.01 (fig. 2A). As shown in fig. 2B, HA-OUR-NLC had a mean zeta potential of -22.87±0.97 mV, matching the condition of within 30 mv (Brgles *et al.*, 2008).

Total entrapment efficiency and drug loading were 45.67±1.14% and 8.76±0.95%, respectively. In addition, transmission electron microscopic imaging of the HA-OUR-NLC (fig. 2C) indicated that these particles were uniform, in the nano-size range and of spherical core shell morphologically.

In vitro release

The four release curves shown in fig. 3 indicated that Rg3 was released more slowly than OA and UA from HA-

OUR-NLC, perhaps because of a higher molecular weight compared with OA and UA. The release rates of OA, UA and Rg3 from HA-OUR-NLC followed the sustained-release Higuchi equations and can be expressed by the following equations: Q_{OA}=5.793+9.66tl/2, R2=0.988; Q_{OU}=5.732+8.748$t^{l/2}$, R^2=0.985; Q_{Rg3}=-0.139-2.585$t^{l/2}$, R^2=0.976 with the drugs incorporated released in a sustained manner via diffusion or degradation (Gajendiran *et al.*, 2013).

Pharmacokinetic properties and tissue distribution

With peak area of OA and UA as ordinate, respective concentration C (μg/mL) of OA and UA as the abscissa, linear regression was performed with the weighted least square method and the standard curve equation of OA and UA was obtained: Y=5287.0X+37332 (R2=0.9996), Y=5793.3X+49450(R2=0.9997).Within the concentration range of 5.04μg/mL ～ 130.10μg/mL of OA, 5.03 μg/mL～130.78μg/mL of UA, both the concentration and the peak area have a good linear relationship.

With peak area of Rg3 as ordinate, concentration C (μg/mL) as the abscissa, linear regression was performed with the weighted least square method, and the standard curve equation of Rg3 was obtained: Y=6001.4X+53311 (R^2=0.9997). Within the concentration range of 4.01μg/mL～150.30μg/mL, both the concentration and the peak area have a good linear relationship.

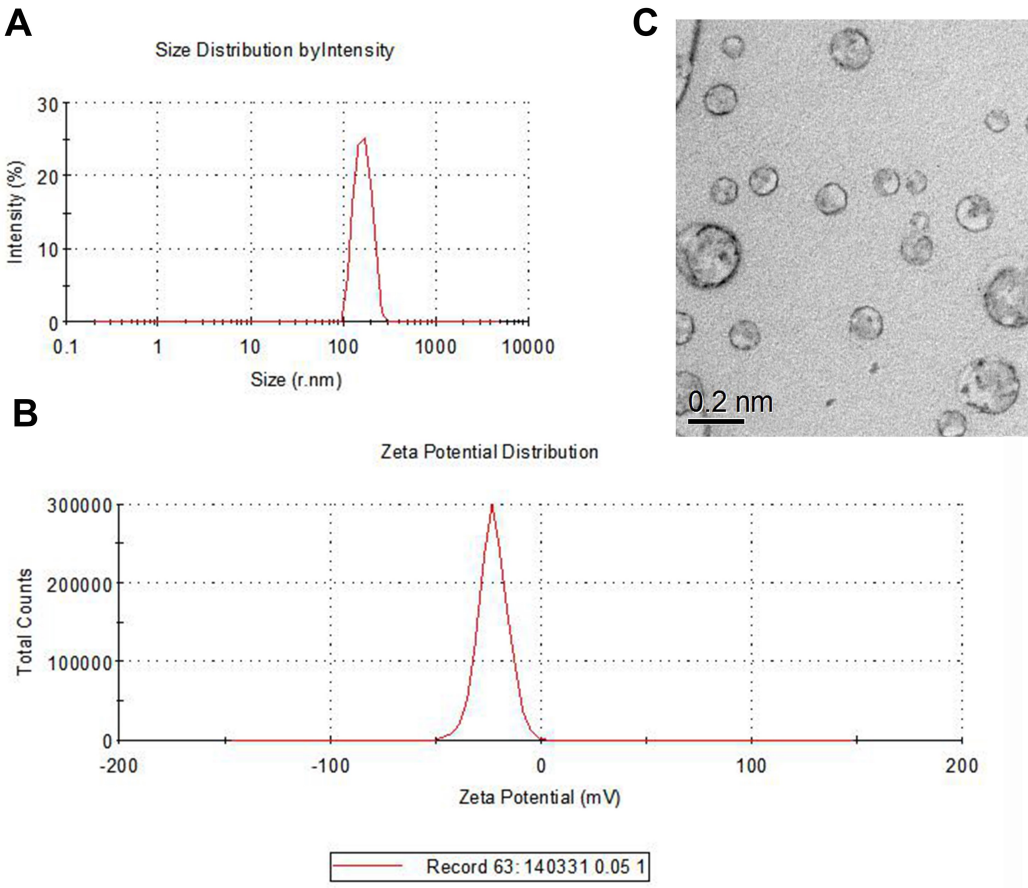

Fig. 2: Particle size distribution (A), zeta potential distribution (B), and transmission electron microscopy (C)（×43000）of HA-OUR-NLC lyophilized powder.

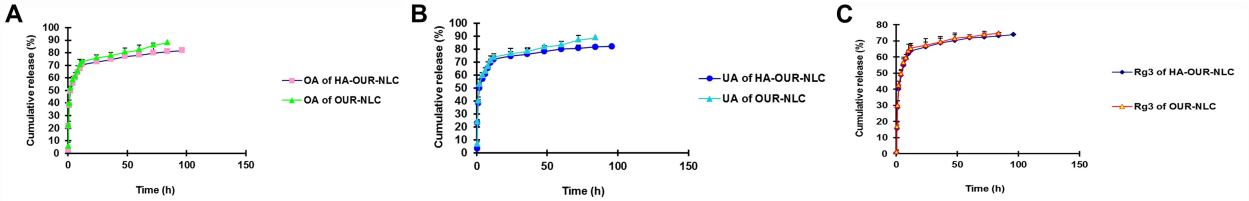

Fig. 3: *In vitro* release curves for OA (A) , UA (B) and Rg3 (C) from HA-OUR-NLC and OUR-NLC in phosphate-buffered solution (pH 7.4) at 37°C. Data are mean ± SD (n = 3).

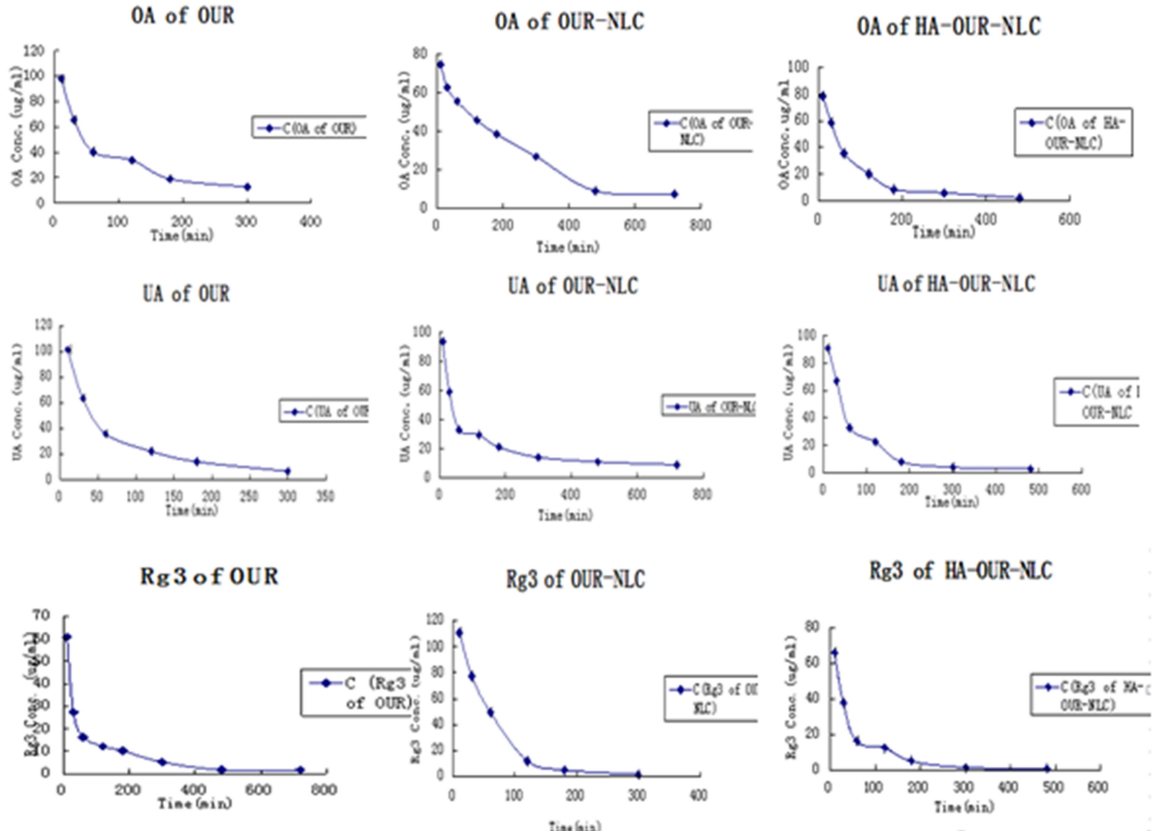

Fig. 4: Plasma concentration–time curves for OA, UA and Rg3 after intravenous administration of OUR, OUR-NLC and HA-OUR-NLC (n=6).

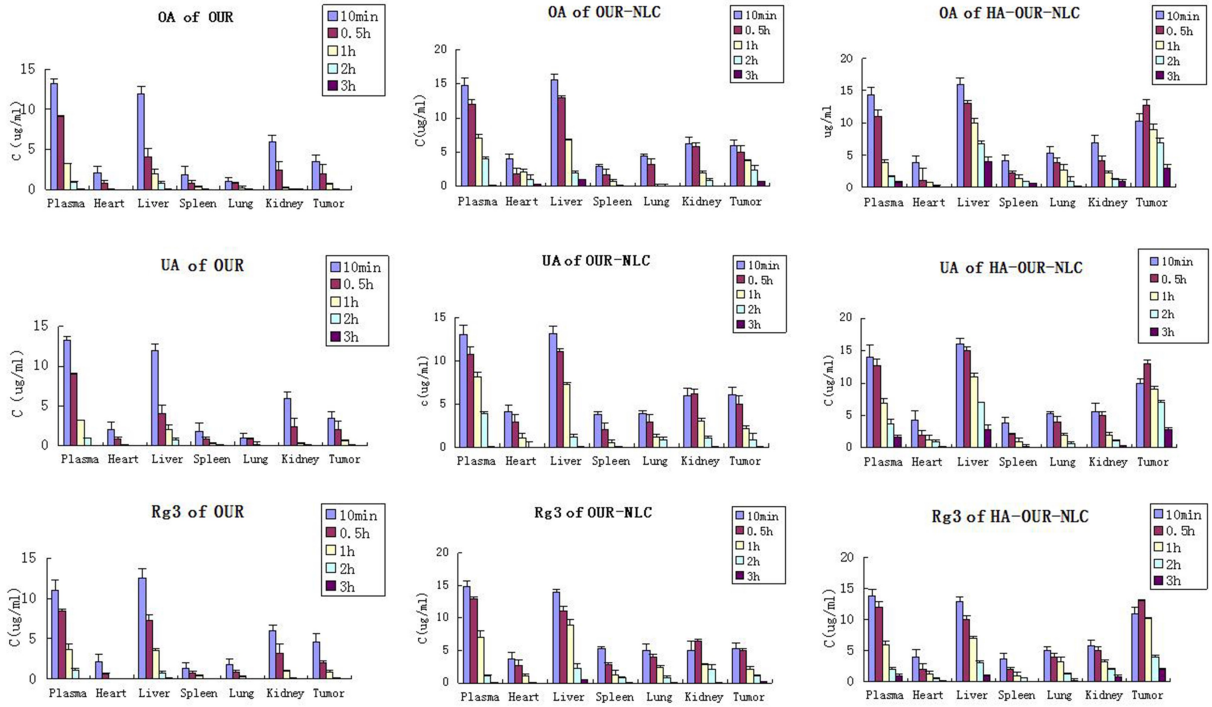

Fig. 5: Biodistribution of OA, UA, and Rg3 from OUR solutions; OA, UA, and Rg3 from OUR-NLC; OA, UA, and Rg3 from HA-OUR-NLC. Organ and blood samples were collected at 10 min' 0.5h' 1h' 2h' and 3h after intravenous injection (n=6).

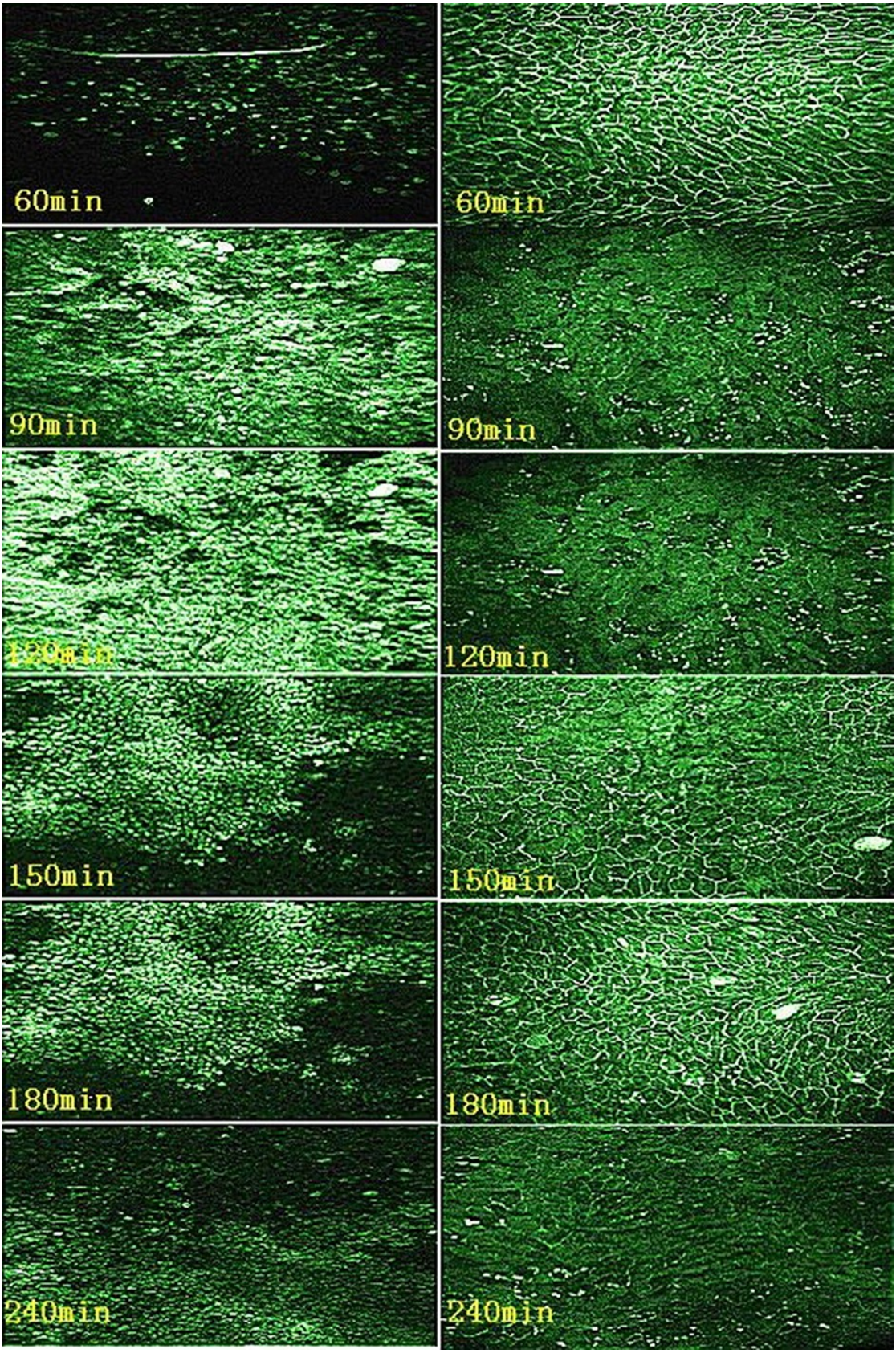

Fig. 6: Images at different times after i.v. administration of FITC-HA-OUR-NLC in tumors and the liver.

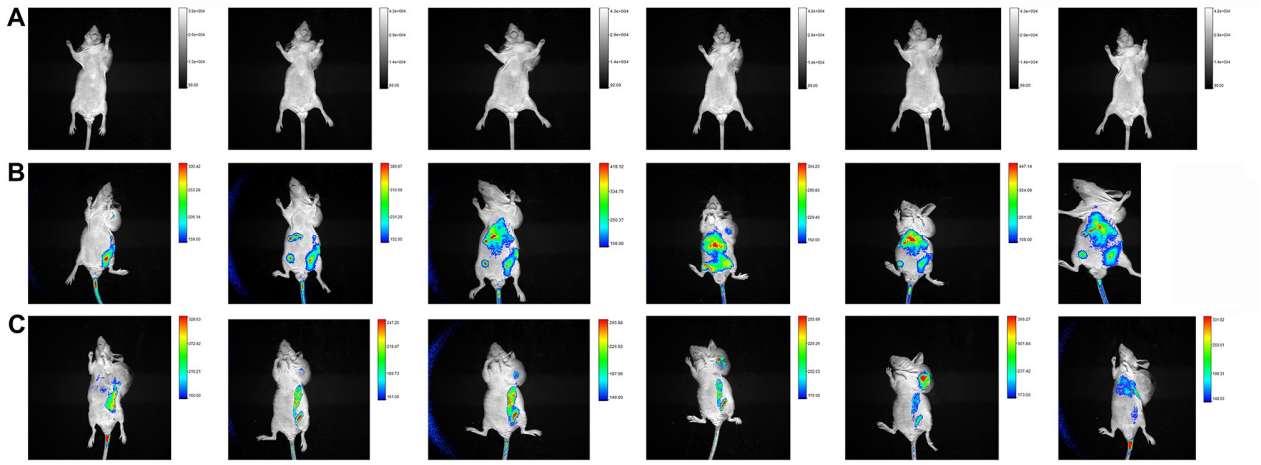

Fig. 7: *In vivo* near-infrared fluorescence imaging of tumors (A, Saline; B, OUR-NLC; C, HA-OUR-NLC)

Blood concentrations of OA, UA and Rg3 were evaluated in healthy SD rats. Blood concentration–time profiles of the drugs and HA-OUR-NLC are shown in fig. 4 and fit a two-compartment model. The initial drug concentrations of OA, UA and Rg3 were higher in OUR than in HA-OUR-NLC and OUR-NLC. However, these three components were rapidly cleared from the circulation in OUR compared with HA-OUR-NLC and OUR-NLC.

The $AUC_{0-\infty}$ of HA-OUR-NLC was significantly higher than that of OUR-NLC. Specifically, AUC values for OA, UA and Rg3 in the HA-OUR-NLC group were 1.67, 1.76 and 1.75 times those of the OUR-NLC group, respectively. These findings indicated that absorption of the three components increased significantly. The significant differences in beta elimination half-life and clearance rate indicates slower elimination in HA-OUR-NLC, with longer circulation time, compared with OUR-NLC.

The percentages of injected dose per gram of tissue in different organs at various time intervals are shown in fig. 5.

Fluorescence in vivo endomicroscopy findings

Eighteen SMMC-7721-bearing female BALB/C-nu nude mice were assessed by FIVE after tail vein injection of HA-OUR-NLC. As shown in fig. 6, FITC-HA-OUR-NLC moved from the extra cellular region gradually to the inside of the cell. After 60 min, the amounts increased gradually, with a positive correlation. After 90 min, they were distributed in the intercellular space, before moving inward to the inner membrane. At 120 min, they moved into the cell and accumulated to a large extent. Thus, FITC-HA-OUR-NLC can deliver drugs in the cell.

Optical in vivo imaging data

DiR-HA-OUR-NLC were obviously localized in the tumor region, as reflected by strong fluorescence signals. Compared with that of DiR-OUR-NLC, the volume of DiR-HA-OUR-NLC was larger in the tumor at 3h (fig. 7); however, the DiR-OUR-NLC group only showed bright systemic signals, and tumor localization was weak. These findings indicated that HA-OUR-NLC can accumulate in the tumor site, in line with our expectations.

In vivo antitumor efficacy

Antitumor efficacy was evaluated in SMMC-7721-bearing female BALB/C-nu nude mice after intravenous administration of N.S at a dose of 0.2 ml or 5-Fu (positive control) at 500g/m^2; the HA-OUR-NLC, OUR-NLC and OUR groups were treated at 0.3 mg/ml. As shown in fig. 8, HA-OUR-NLC showed overt antitumor effects. Similar to the 5-Fu group, the HA-OUR-NLC treatment group showed significantly smaller tumors compared with N.S. control treated mice. However, the tumors treated with OUR and OUR-NLC were similar to those of the N.S. group.

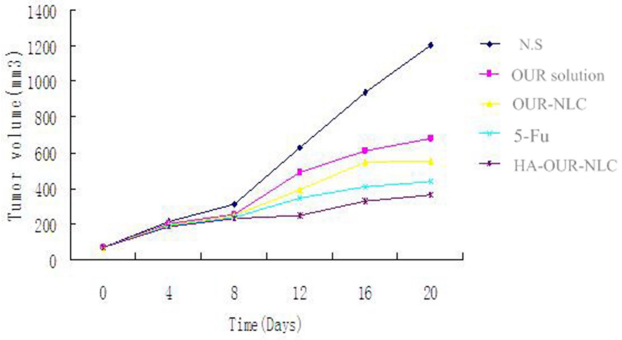

Fig. 8: Time course of tumor volumes (n=5).

Tumor histology and weight measurements demonstrated that HA-OUR-NLC had an excellent antitumor activity (fig. 9). Compared with the 5-Fu, OUR-NLC, OUR, and N.S. groups, the HA-OUR-NLC group showed significantly lower tumor weights.

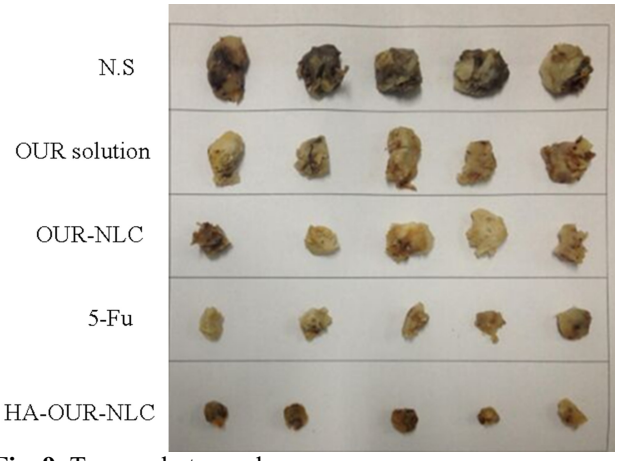

Fig. 9: Tumor photographs

H&E staining (fig. 10) showed that after treatment with HA-OUR-NLC, the tumor cells shrunk; the nuclei were hyperchromatic with condensed chromatin, representing typical apoptotic morphological changes. These results indicated that HA-OUR-NLC have obvious inhibitory effects on tumor growth. After treatment with HA-OUR-NLC, overtly less vessels were found in the tumor tissues (fig. 11). These results indicated that modification of nanostructured lipid carriers plays a role in angiogenesis inhibition in tumor tissues.

DISCUSSION

The cationic HA-OUR-NLC were prepared by the charge adsorption technology. The results showed that the entrapment efficiencies (EE) of OA and UA were similar and the reason may be that OA and UA are isomers. However, these values were higher than that of Rg3 irrespective of the other factors. We thought the cause might be the core-shell structure of HA-OUR-NLC. As the aglycones, molecular weight and volume of OA and UA are smaller than Rg3. Therefore it is easier to encapsulated in nanoparticles or adsorbed on the surface of nanoparticles causing higher EE. In addition, there is a competitive relationship between OA, UA and Rg3 in the process of carrying drugs. In the limited carrier materials, the ability to carry drugs is also limited. Therefore, when changing the dosage of the drug and the proportion of the three components, the entrapment efficiency and drug loading of the three components are affected. This may be explained by the different drug molecular weights; indeed, OA (456.71 Da) and UA (456.68 Da) are smaller than Rg3 (784.30 Da), and easier to bind to nanoparticles.

In vitro release assessment was performed by the dialysis method. As shown in fig. 3, release rates of OA, UA and Rg3 from HA-OUR-NLC were slower than those from OUR-NLC. Cumulative amounts of these three components stably released over 70h were above 70%. This might be explained by the fact that the HA-OUR-NLC nanoparticles had a core-shell structure.

According to the similarity-intermiscibility theory, the solubility of OA and UA in ethanol is higher than Rg3 because OA and UA are isomers and low polar molecules while Rg3 is saponin and high polar molecule. Thus Rg3 may have a little precipitation that is not easily wrapped in the process of preparing multicomponent nanoparticles. The vitro release of OUR-NLC includes three stages: exfoliation, pore diffusion release and carrier degradation.At 96h, the release degree of OA and UA was above 80%, and Rg3 release was about 70%.The reason may be: (1)Saponins are encapsulated in the nucleus of nanoparticles due to its big molecular weight and larger volume while the glycosides are not only encapsulated in nanoparticles but may also be adsorbed on the surface of nanoparticles. (2) glycosides which are small molecular weight and small volume are easier to diffuse from nanoparticles.
On the study of Pharmacokinetic properties and tissue distribution, As expected, OA, UA, and Rg3 levels were higher in the tumors for HA-OUR-NLC compared with OUR, due to the higher efficiency of nanoparticles predominantly by virtue of enhanced permeability.

The concentrations of the above three components in the HA-OUR-NLC and OUR-NLC groups were higher in the liver, spleen and lung, compared with OUR group values. This may be due to NLC size and the EPR effect of HA-OUR-NLC in the tumor. Furthermore, HA-OUR-NLC resulted in significantly higher accumulation of OA, UA and Rg3 in the tumor than did OUR-NLC. This indicated HA-OUR-NLC has a certain tumor targeting property.

The research results show that the HA-OUR-NLC and OUR-NLC changed its pharmacokinetic parameters, compared with the solution. In addition, there is a significant difference in T1/2β' AUC and plasma clearance ($P<0.05$ or $P<0.01$). It shows that the half-life and retention time of the drug in the body were prolonged by making the nanoparticles from OA, UA and Rg3, and the bioavailability was improved.

Furthermore, the pharmacokinetic parameters is better than OUR–NLC after modified by HA. It can significantly prolong the half-life and retention time of drugs in rats, reduce the clearance rate significantly, greatly improve the bioavailability of drugs and play a long-term role.

After tail vein injection, compared with FITC-OUR-NLC, the fluorescence intensity of the tumor site of HA-OUR-NLC increased with the time, and the nanoparticles are gradually infiltrated into the cell from outside by the number of nanoparticles gradually increasing.

This indicates that the number of nanoparticles entering the cell is positively correlated with time. Therefore, this

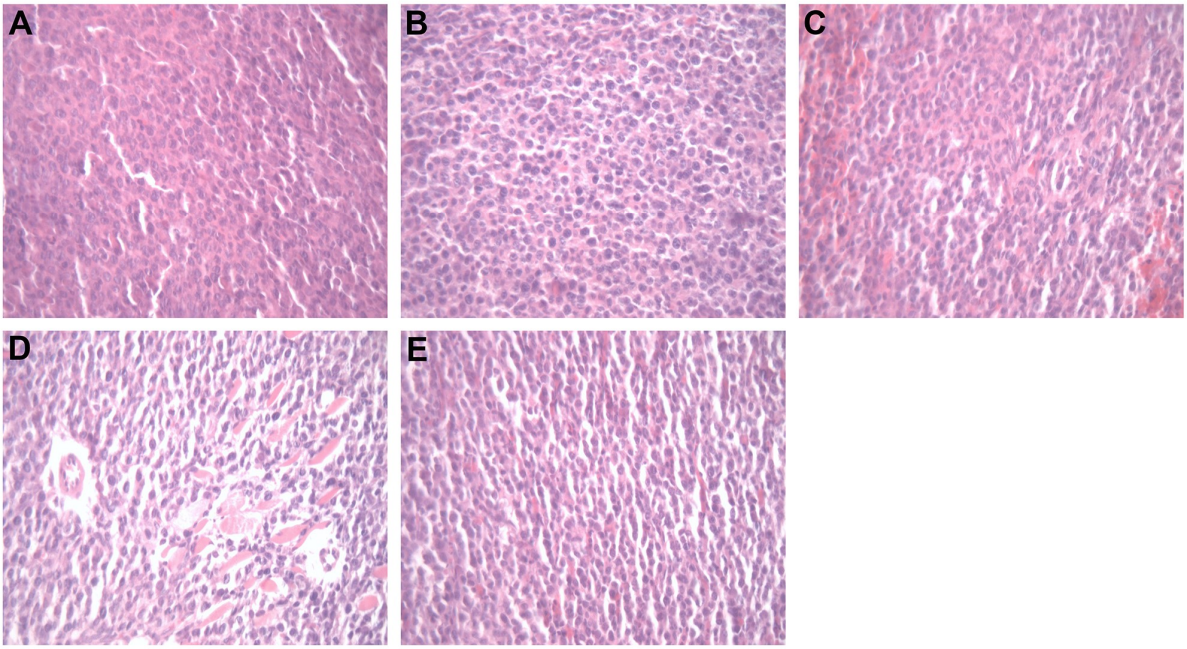

Fig. 10: Pathological sections (×100; A, model group; B, OUR group; C, OUR-NLC group; D, HA-OUR-NLC group; E, Positive control group)

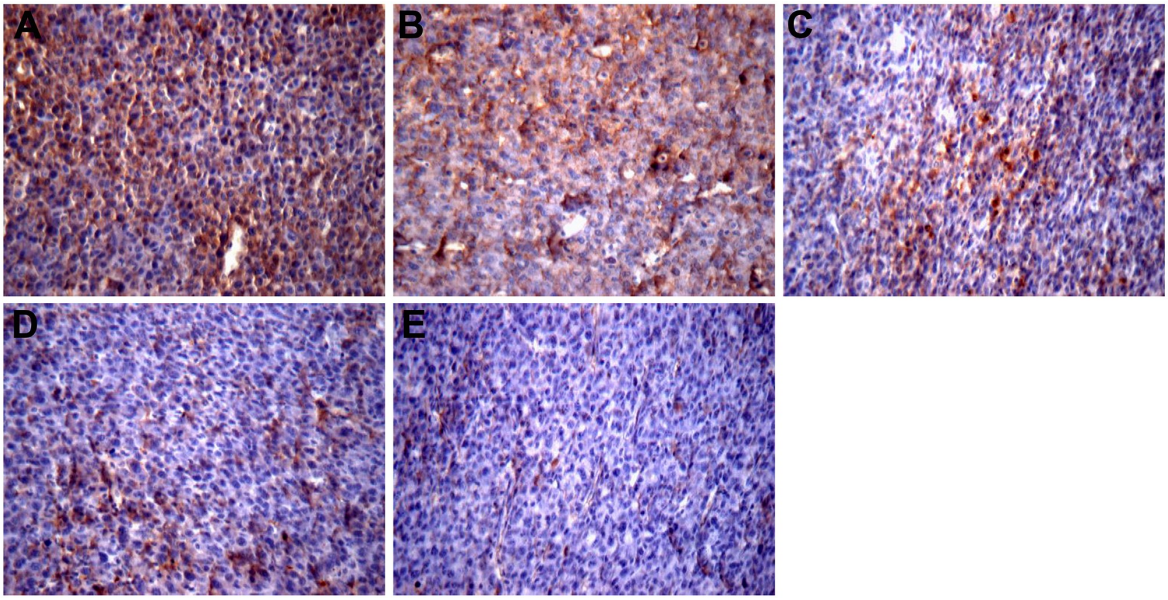

Fig. 11: Pathological sections (×400; A, modal group; B, OUR group; C, OUR-NLC group; D, Positive control group; E, HA-OUR-NLC group).

experiment not only confirms that NLC can reach the tumor, but also can enter the tumor cells after HA modification, which reflects the characteristics of the active target tumor cells.

In this study, hyaluronic acid was modified by charge adsorption on the surface of NLC, hoping to give it the ability to target tumor cells. This ability is expressed in the presence of relatively normal cells on the surface of tumor cells expressing more CD44 molecules, Through CD44 mediated endocytosis, the tumor cells can be more specific in the uptake of nano-lipid carriers. Tumor cells can be more specifically ingest NLC by CD44 mediated endocytosis. Compared with OUR-NLC, HA-OUR-NLC group has stronger tumor targeting effect. It was further verified that the NLC modified by HA had good tumor targeting effect, which was in line with the expected hypothesis.

These results are accordant with fluorescence in vivo

endomicroscopy finding, and further verify the effectiveness of initiative targeting of HA-OUR-NLC.

In this study, we aimed to develop an HA coated nanostructured lipid carrier delivery system for targeting OUR to tumor cells with CD44 over expression. HA-OUR-NLC were successfully prepared using the solvent ultrasonic dispersion method and electrostatic attraction. During electrostatic attraction, the high positive zeta potential of OUR-NLC, low concentration of HA, and excessive amounts of HA were essential for HA-OUR-NLC stability. The physicochemical properties of HA-OUR-NLC were characterized in detail, with *in vitro* drug release patterns showing relatively prolonged drug release. Because of significant changes in pharmacokinetic parameters, HA-OUR-NLC have the potential to increase the bioavailability of the three seed components, with a sustained-release effect, indicating a certain tumor targeting property for the HA-OUR-NLC. Meanwhile, FIVE and OIVI data indicated that HA-OUR-NLC could deliver drugs in the cell, accumulating in the tumor site, as expected.

CONCLUSION

We successfully prepared HA-OUR-NLC and optimized its process. The appearance was light blue emulsion, and the total encapsulation rate and total load were (45.67 + 1.14) % and (8.76 + 0.95) %.The optimization results are good.

The HA-OUR-NLC characteristics were studied. The HA-OUR-NLC has a uniform shape, uniform distribution, particle size and PDI value of 165.15±3.84 nm and 0.227±0.01 and Zeta potential is -22.87±0.97 mV. In vitro release behavior fit the Higuchi equation, which has a certain sustained release effect.

Pharmacokinetic research results as follows: HA-OUR-NLC changed its pharmacokinetic parameters and prolonged the half-life and residence time of drugs significantly. In addition, the clearance rate was obviously reduced, the AUC value was increased and the liver function is prolonged. HA-OUR-NLC improve the bioavailability of the drug and play a long-term effect. OUR-NLC We have successfully evaluated the target ability. Compared with OUR-NLC, HA-OUR-NLC group showed stronger tumor targeting ability. The FIVE results showed that HA-OUR-NLC could transfer drugs to liver cells; The OIVI results showed that the fluorescence intensity of the tumor site in the DiR-HA-OUR-NLC group was significantly stronger than that of the DiR-OUR-NLC group at 6 points and the characteristics of the target were verified.

The results of pharmacodynamics in vivo showed that, with the influence of HE staining and tumor micro vascular density, HA-OUR-NLC had a significant inhibitory effect on tumor in tumor mice. Furthermore, HA-OUR-NLC showed more pronounced antitumor efficacy than OUR-NLC and OUR in SMMC-7721-bearing female BALB/C-nu nude mice. The mechanisms may be as follows: (1) HA-OUR-NLC enhanced the intracellular uptake of OUR with more overt antitumor efficacy because of HA recognition by CD44 on the tumor cell surface; (2) OUR release was delayed by HA-OUR-NLC, increasing drug half-life as well as the drug amounts in tumor tissues.

Overall, these findings support the development of NLC co-loaded simultaneously with multiple components of different characteristics. HA-OUR-NLC constitute a promising formulation for prolonging drug circulation time, and can be targeted to tumor cells and tissues. This study provides insights into methods and techniques for designing nanoparticle drug delivery systems for multicomponent traditional Chinese medicine preparations.

ACKNOWLEDGMENTS

Shuang Sun and Qingxia Guan contributed equally to this work. First author Shuang Sun is postdoctoral fellow of Heilongjiang University of Traditional Chinese Medicine. The authors are grateful for the grants received in support of this research from the Natural Science Foundation of Heilongjiang Province (H2016060), the National Natural Science Foundation of China (81803985), the Natural Science Foundation of Heilongjiang Province (H2016076), the Outstanding and Innovative Talents Foundation of Heilongjiang University of Chinese Medicine (Academic Leader Foundation 2012) and Research Fund Project of Heilongjiang University of Traditional Chinese Medicine (201408).

REFERENCES

Brgles M, Jurasin D, Sikiric MD, Frkanec R and Tomasic J (2008). Entrapment of ovalbumin into liposomes-factors affecting entrapment efficiency, liposome size, and zeta potential. *J. Liposome Res.,* **18**(3): 235-248.

Chen H, Li KY, Chen F and Yan HM (2012). Establishment of xenograft mouse models for studying human hepatocellular carcinoma by using vivo imaging system. *Journal of Lanzhou University (Medical Science),* **38**(1): 11-15.

Danhier F, Vroman B, Lecouturier N, Crokart N, Pourcelle V, Freichels H, Jerome C, Marchand-Brynaert J, Feron O and Preat V (2009). Targeting of tumor endothelium by RGD-grafted PLGA-nanoparticles loaded with paclitaxel. *J. Control Release,* **140**(2): 166-173.

De Stefano I, Battaglia A, Zannoni GF, Prisco MG, Fattorossi A, Travaglia D, Baroni S, Renier D, Scambia

G, Ferlini C and Gallo D (2011). Hyaluronic acid-paclitaxel: Effects of intraperitoneal administration against CD44(+) human ovarian cancer xenografts. *Cancer Chemoth. Pharm.,* **68**(1): 107-116.

Gajendiran M, Gopi V, Elangovan V, Murali RV and Balasubramanian S (2013). Isoniazid loaded core shell nanoparticles derived from PLGA-PEG-PLGA tri-block copolymers: *in vitro* and *in vivo* drug release. *Colloids Surf B Biointerfaces,* **104**(1): 107-115.

Han YY, Xue XW, Shi ZM, Wang PY, Wu XR and Wang XJ (2014). Oleanolic acid and ursolic acid inhibit proliferation in transformed rat hepatic oval cells. *World J. Gastroenterol,* **20**(5): 1348-1356.

Helms S (2004). Cancer prevention and therapeutics: Panax ginseng. *Altern. Med. Rev.,* **9**(3): 259-274.

Heo DN, Yang DH, Moon HJ, Lee JB, Bae MS, Lee SC, Lee WJ, Sun IC and Kwon IK (2012). Gold nanoparticles surface-functionalized with paclitaxel drug and biotin receptor as theranostic agents for cancer therapy. *Biomaterials.,* **33**(3): 856-866.

Igami K, Shimojo Y, Ito H, Miyazaki T and Kashiwada Y (2015). Hepatoprotective effect of fermented ginseng and its major constituent compound K in a rat model of paracetamol (acetaminophen)-induced liver injury. *J. Pharm. Pharmacol.,* **67**(4): 565-572.

Jain S, Rathi VV, Jain AK, Das M and Godugu C (2012). Folate-decorated PLGA nanoparticles as a rationally designed vehicle for the oral delivery of insulin. *Nanomedicine (Lond),* **7**(9): 1311-1337.

Li JS, Deng DW and Zeng LJ (2016). Forkhead Box Q1 Promotes Proliferation of SMMC-7721 Hepatocellular Carcinoma Cells. *Chin. J. Biochem. Mol. Biol.,* **32**(4): 446 -451.

Li WT, Zhao FM and Zhou HG (2016). Effects of Xiao'ai Jiedu Formula drug-containing serum on telomerase and apoptosis-related mRNA expression in human hepatoma SMMC-7721 cells. *Chin. J. Tradit. Chin. Med. Pharm.,* **31**(4): 1211-1214.

Liu D, Liu F, Liu Z, Wang L and Zhang N (2011a). Tumor specific delivery and therapy by double-targeted nanostructured lipid carriers with anti-VEGFR-2 antibody. *Mol Pharm.,* **8**(6): 2291-2301.

Liu D, Liu Z, Wang L, Zhang C and Zhang N (2011b). Nanostructured lipid carriers as novel carrier for parenteral delivery of docetaxel. *Colloids Surf B Biointerfaces,* **85**(2): 262-269.

Luan J, Zhang D, Hao L, Qi L, Liu X, Guo H, Li C, Guo Y, Li T, Zhang Q and Zhai G (2014). Preparation, characterization and pharmacokinetics of Amoitone B-loaded long circulating nanostructured lipid carriers. *Colloids Surf B Biointerfaces.,* **114**(1): 255-260.

Niranjana Murthy H, Dandin VS and Yoeup Paek K (2014). Hepatoprotective activity of ginsenosides from Panax ginseng adventitious roots against carbon tetrachloride treated hepatic injury in rats. *J. Ethnopharmacol.,* **158 Pt A**(2): 442-446.

Oh GS, Yoon J, Lee GG, Oh WK and Kim SW (2015). 20(S)-protopanaxatriol inhibits liver X receptor alpha-mediated expression of lipogenic genes in hepatocytes. *J. Pharmacol. Sci.,* **128**(2): 71-77.

Shamma RN and Aburahma MH (2014). Follicular delivery of spironolactone via nanostructured lipid carriers for management of alopecia. *Int. J. Nanomedicine,* **9**(1): 5449-5460.

Wang CZ, Aung HH, Ni M, Wu JA, Tong R, Wicks S, He TC and Yuan CS (2007). Red American ginseng: ginsenoside constituents and antiproliferative activities of heat-processed Panax quinquefolius roots. *Planta Med.,* **73**(7): 669-674.

Wang MT, Jin Y, Yang YX, Zhao CY, Yang HY, Xu XF, Qin X, Wang ZD, Zhang ZR, Jian YL and Huang Y (2010). *In vivo* biodistribution, anti-inflammatory and hepatoprotective effects of liver targeting dexamethasone acetate loaded nanostructured lipid carrier system. *Int. J. Nanomedicine,* **5**(1): 487-497.

Wu XG, Zhu DH and Li X (2001). Anticarcinogenic effect of red ginseng on the development of liver cancer induced by diethylnitrosamine in rats. *J. Korean Med. Sci.,* **16**(Suppl): S61-65.

Yang A, Yang L, Liu W, Li Z, Xu H and Yang X (2007). Tumor necrosis factor alpha blocking peptide loaded PEG-PLGA nanoparticles: Preparation and *in vitro* evaluation. *Int. J. Pharm.,* **331**(1): 123-132.

Yang XY, Li YX, Li M, Zhang L, Feng LX and Zhang N (2013). Hyaluronic acid-coated nanostructured lipid carriers for targeting paclitaxel to cancer. *Cancer Lett.,* **334**(2): 338-345.

Zhan C, Gu B, Xie C, Li J, Liu Y and Lu W (2010). Cyclic RGD conjugated poly(ethylene glycol)-co-poly (lactic acid) micelle enhances paclitaxel anti-glioblastoma effect. *J. Control Release,* **143**(1): 136-142.

Zhang K, Lv S, Li X, Feng Y, Li X, Liu L, Li S and Li Y (2013). Preparation, characterization, and *in vivo* pharmacokinetics of nanostructured lipid carriers loaded with oleanolic acid and gentiopicrin. *Int. J. Nanomedicine,* **8**(1): 3227-3239.

Zhao P, Wang H, Yu M, Cao S, Zhang F, Chang J and Niu R (2010). Paclitaxel-loaded, folic-acid-targeted and TAT-peptide-conjugated polymeric liposomes: *in vitro* and *in vivo* evaluation. *Pharm. Res.,* **27**(9): 1914-1926.